Materials Today Chemistry 35 (2024) 101867

Contents lists available at ScienceDirect

Materials Today Chemistry

journal homepage: www.journals.elsevier.com/materials-today-chemistry/

Tailoring the electrical conductivity of Poly(vinylidene fluoride) by blending with poly (3,4-ethylenedioxythiophene) Polystyrene sulfonate (PEDOT:PSS) and ionic liquids

Luis Amaro Martins [a], Laura Teruel Biosca [a], Roser Sabater i Serra [a,b], Andreu Andrio Balado [c], José Antonio Gómez-Tejedor [a,b], Daniela M. Correia [d], Liliana Fernandes [e], Carlos M. Costa [e,f,g,*], Senentxu Lanceros-Méndez [e,f,h,i], José Luis Gomez Ribelles [a,b], Isabel Tort-Ausina [a,b]

[a] Centre for Biomaterials and Tissue Engineering, CBIT, Universitat Politècnica de València, 46022 Valencia, Spain
[b] Biomedical Research Networking Center on Bioengineering, Biomaterials and Nanomedicine (CIBER-BBN), Valencia, Spain
[c] Departamento de Física, Universitat Jaume I, 12071 Castelló, Spain
[d] Centre of Chemistry, University of Minho, 4710-057 Braga, Portugal
[e] Physics Centre of Minho and Porto Universities (CF-UM-UP), University of Minho, 4710-057 Braga, Portugal
[f] Laboratory of Physics for Materials and Emergent Technologies, LapMET, University of Minho, 4710-057 Braga, Portugal
[g] Institute of Science and Innovation for Bio-Sustainability (IB-S), University of Minho, 4710-057 Braga, Portugal
[h] BCMaterials, Basque Center for Materials, Applications and Nanostructures, UPV/EHU Science Park, 48940 Leioa, Spain
[i] Ikerbasque, Basque Foundation for Science, 48009 Bilbao, Spain

ARTICLE INFO

Keywords:
PVDF
PEDOT:PSS
Ionic liquids
Dielectric response
Electrical conductivity
Electric modulus

ABSTRACT

In order to tailor dielectric response and electrical conductivity, novel polymer blends based on poly(vinylidene fluoride (PVDF) and different fillers composed by poly(3,4-ethylenedioxythiophene):poly(styrene sulfonate) (PEDOT:PSS), and PEDOT:PSS/ionic liquids (ILs): PEDOT:PSS/N-ethyl-N-methylpyrrolidinium bis(fluorosulfonyl)imide ([C_2mpyr][FSI]) and PEDOT:PSS/N-ethyl-N-methylpyrrolidinium bis(trifluoromethanesulfonyl)imide ([C_2mpyr][TFSI]), with different PEDOT:PSS/IL contents (10, 20 and 40 wt%) were prepared through solvent casting. The morphological, physical-chemical and thermal properties of the polymer blends were evaluated, together with the influence of PEDOT:PSS/IL on the PVDF crystallization kinetics, dielectric and electrical conductivity.

The incorporation of PEDOT:PSS/IL in the polymer matrix lead to a decrease of the PVDF spherulites. Furthermore, it was detected that both PEDOT:PSS and IL act as nucleation agents, promoting the homogeneous crystallization of PVDF as well as the crystallization into its b and g polar phases. The electrical conductivity formalism revealed significant contributions of PEDOT:PSS/IL to the electrical conductivity behavior of the blends, being thermally activated and described by the charge transport mechanism. Further, the dc conductivity increases due to the higher number of charge carriers of the PEDOT:PSS/IL content.

The tailorable electrical characteristics of the PVDF/PEDOT:PSS-IL blends demonstrate their potential for applications in areas such as ionic actuators and battery devices.

1. Introduction

Smart materials are considered responsive materials and/or material systems capable of physical-chemical variations depending on external environmental changes such as, pH, stress, temperature, light, electric or magnetic, among others [1,2]. As for smart material composites, they are generally defined as a combination of materials working synergistically, leading to creating complex interactions that result in improved or novel functional active responses [2].

Polymer-based smart materials are attracting strong interest in various technological areas due to their simple processing and easy device integration, namely in sensors and actuators, among others [3]. Additionally, the inclusion of fillers as active materials such as nanoparticles, ionic liquids (ILs), proteins or carbon nanotubes, among

* Corresponding author. Physics Centre of Minho and Porto Universities (CF-UM-UP), University of Minho, 4710-057 Braga, Portugal.
E-mail address: cmscosta@fisica.uminho.pt (C.M. Costa).

https://doi.org/10.1016/j.mtchem.2023.101867
Received 6 August 2023; Received in revised form 20 November 2023; Accepted 18 December 2023
Available online 21 December 2023

others, allows the possibility of further tailoring their response, as well as the improvement or addition of new functionalities [4].

Amongst the available smart electroactive polymers (EAPs), polyvinylidene fluoride (PVDF) can be easily incorporated in advanced systems due to its chemical stability, high polarity and ionic conductivity [5]. Additionally, PVDF can be easily processed into different shapes and forms, including films, membranes, spheres or fibers [6]. This polymer can crystalize into five different polymorphs (α, β, γ, δ and ε) depending on the processing conditions, the β-phase standing out for being the one with the most polar one and the one with the highest piezoelectric, pyroelectric and ferroelectric response [1]. Due to these properties, PVDF has been used in applications including sensors [7,8], actuators [9,10], tissue engineering [7,11], microfluidic [12,13], environmental [14,15] and energy harvesting and storage [8,16].

Poly(3,4-ethylenedioxythiophene):poly(styrene sulfonate) (PEDOT:PSS) is a conductive EAP often implemented in technological applications [17]. This polymer has been applied successfully in flexible electronics [18,19], hybrid solar cells [20–23], energy storage [24,25], tissue engineering [26,27], bioelectronics [28,29], actuators [30], among others [31–33], due to its high thermal stability and biocompatibility, adjustable conductivity and good transparency to visible light [17].

Recently, PEDOT:PSS has been mixed with different ILs to increase the conductivity, achieving high electronic and ionic conductivities due to the affinity of ILs and conductive polymers [34].

With respect to the combination of PEDOT:PSS with IL, it has been shown that IL anions support the largest amount of charge carriers evenly distributed along the PEDOT backbone to further increase the electrical conductivity [35]. In addition, for PEDOT:PSS solutions with the same imidazolium based cation ($[EMIM]^+$) but varying the anion, the solvation of each ion in water plays a major role in the free energy of ion binding, in which the anions are weakly stabilized by hydration, favoring the ion exchange [36]. Further, cation/anion modification of ILs distinctly improves the electrical conductivity of PEDOT:PSS and the cation/anion modified ILs allow to control the crystallinity and π–π stacking density of conjugated PEDOT chains and the growth of amorphous PSS domains via IL-induced phase separation between PEDOT and PSS [37].

The combination of PVDF with PEDOT:PSS has already been explored to some extent, mostly by using PEDOT:PSS as a conductive/electrode layer in device fabrication, or less frequently as filler to increase the PVDF polymer conductivity [31,38–42]. On the other hand, there are no reports on PVDF blends with PEDOT:PSS, considering the relevant role of their miscibility. However, the understanding of the properties comprising PVDF/PEDOT:PSS blends films is still a work under development, with only a few recent works reporting on this system [38,42,43].

Taking the previously mentioned into consideration, this work reports on the development of novel PVDF-based blends with PEDOT:PSS/[C2mpyr][FSI] (N-ethyl-N-methylpyrrolidinium bis(fluorosulfonyl) imide) and PEDOT:PSS/[C2mpyr][TFSI] (N-ethyl-N-methylpyrrolidinium bis(trifluoromethanesulfonyl)imide) as fillers, allowing to tailor the electrical properties of the materials. The films were processed by solvent casting with different IL contents up to 40 wt%. The PVDF/PEDOT:PSS/IL blends morphology, physical-chemical, thermal and electrical properties were studied. The electrical conductivity spectra were evaluated through broadband dielectric spectroscopy (BDS), as an essential issue for applications that require tailored ionic conductivity.

2. Experimental section

2.1. Materials

Poly(vinylidene fluoride) (PVDF, Solef 6010, Mw = 300–320 kDa), N,*N*-dimethylformamide (DMF, 99.5 %), PEDOT:PSS aqueous solution (Clevios PH1000) and the ionic liquids, (N-ethyl-N-methylpyrrolidinium bis(fluorosulfonyl)imide), C_2mpyrFSI, and *N*-ethyl-*N*-methylpyrrolidinium bis(trifluoromethanesulfonyl)imide), C_2mpyrTFSI, were purchased from Solvay, Merck, Heraeus and Iolitec, respectively.

Table 1
wt ratio of each component in the blend samples.

	PVDF wt. %	PEDOT:PSS wt.%	[C2mpyr][FSI] wt.%	[C2mpyr][TFSI] wt.%
PVDF	100	–	–	–
Blend FSI 10	90	7	3	–
Blend FSI 20	80	14	6	–
Blend FSI 40	60	28	12	–
Blend TFSI 40	60	28	–	12

2.2. Preparation of the PVDF blends with PEDOT:PSS and ionic liquids

PVDF blends comprising PEDOT:PSS/[C_2mpyr][FSI] and PEDOT:PSS/[C_2mpyr][TFSI], the latter with electrical conductivity values of 18.13 and 22.8 S m^{-1}, respectively, as obtained from the I–V curves, were prepared by solvent casting. In a first step, a mixture of PEDOT and the IL [C2mpyr][FSI] or [C2mpyr][TFSI] in a 70/30 wt ratio were dissolved (EtOH) with a concentration of 22.5gL^{-1}. A second solution was prepared with PVDF/DMF at 15/85 wt % ratio. In a second step, different contents of the PEDOT:PSS/IL solutions (10, 20 and 40 wt%) were dispersed on DMF. After that, the PEDOT:PSS/IL/DMF were mixed and magnetically stirred with the PVDF/DMF solution in a variable ratio that leads to the final weight content of PVDF in the film being 90, 80 or 60 wt%. Then, the solutions were spread onto glass substrates followed by solvent evaporation at 210 °C (above PVDF melting temperature) in an oven (P-Select) for 10 min [6]. The blends will be identified henceforth as abbreviation of anion (FSI or TFSI) and the filler content (10, 20 and 40 %). The composition of the samples is shown in Table 1. In the series containing [C2mpyr][FSI] as IL, the relationship between PEDOT and IL remains constant.

2.3. Characterization techniques

The microstructure of the blend samples was analyzed using a field emission scanning electron microscope (FESEM; ZEISS Ultra-55 at 30 kV, 500 pA), following the deposition of a conductive platinum layer.

Differential Scanning Calorimetry (DSC) was performed in approximately 7.5 mg samples using a PerkinElmer DSC 8000 at a heating rate of 20 °C/min, under a flowing nitrogen atmosphere. The analysis was conducted between 50 °C and 200 °C.

Fourier Transform Infrared (FTIR) measurements in the attenuated total reflection (ATR) mode were carried out using a Jasco 4100 spectrometer from 400 to 4000 cm^{-1} with a resolution of 4 cm^{-1}. The spectra were obtained after 64 scans. In the blends containing three phases (α+β+γ), the relative fraction of the phases was determined using equation (1) [44,45]:

$$F_{EA} = \frac{I_{EA}}{\left(\frac{k_{840}}{k_{763}}\right)(I_{763} + I_{EA})} \times 100\% \quad (1)$$

where I_{EA} and I_{763} represent the absorbance at 840 and 763 cm^{-1}, and k_{763} and k_{763} are the absorption coefficients for the above frequencies (6.1×10^4 and 7.7×10^4 cm^2 mol^{-1}, respectively).

The β-phase (F(β)) and γ-phase (F(γ)) content in the samples were calculated using the following equations [45]:

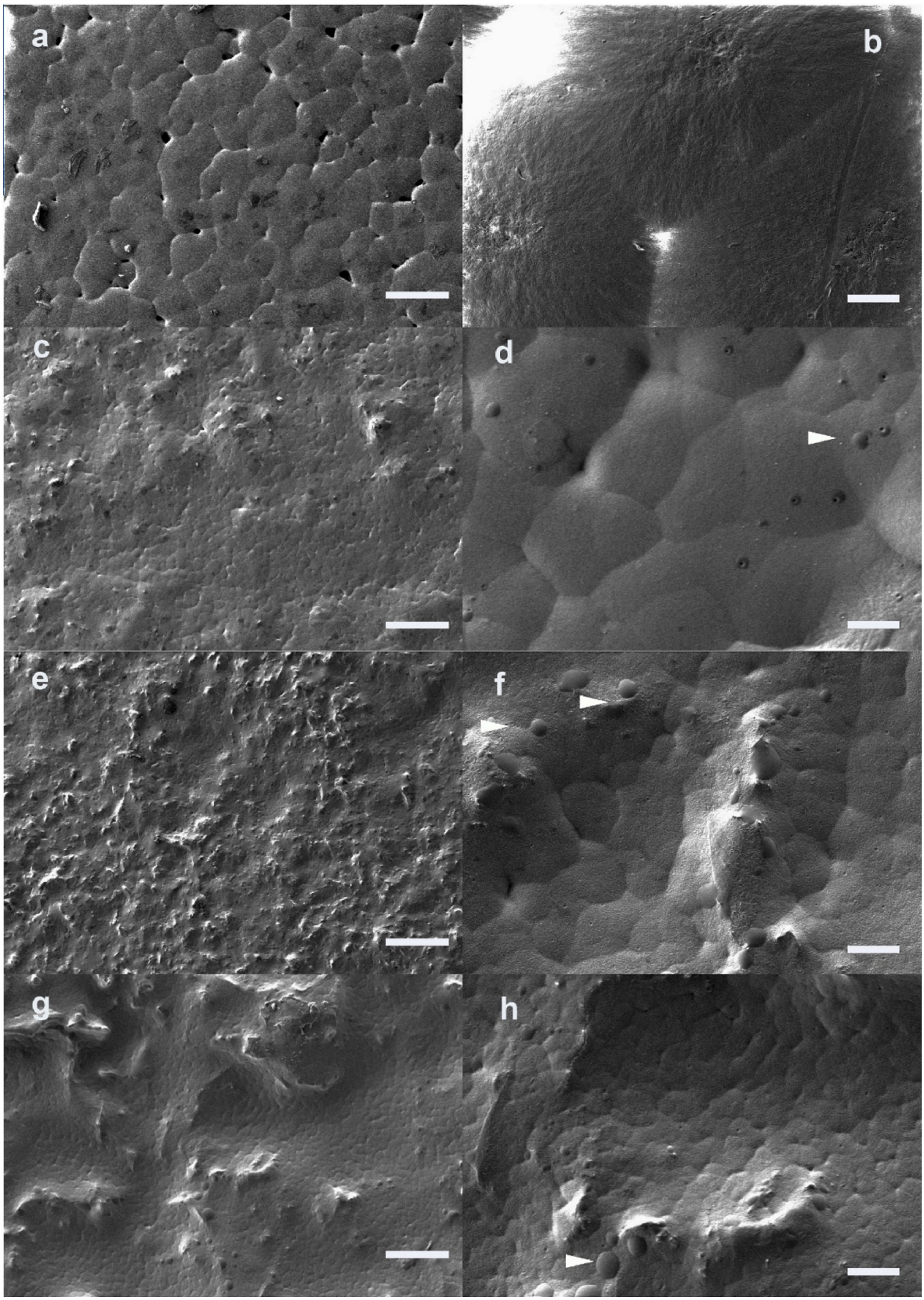

Fig. 1. FESEM images. (a,b) PVDF, (c,d) Blend FSI20, (e,f) Blend FSI40 (g,h) Blend TFSI40. The scale bar shown in (a,c,e,g) corresponds to 40 μm, while the one in (b, d,f,h) corresponds to 4 μm. The arrows indicate circular-shaped aggregates that are associated with IL droplets secreted at the surface of the sample.

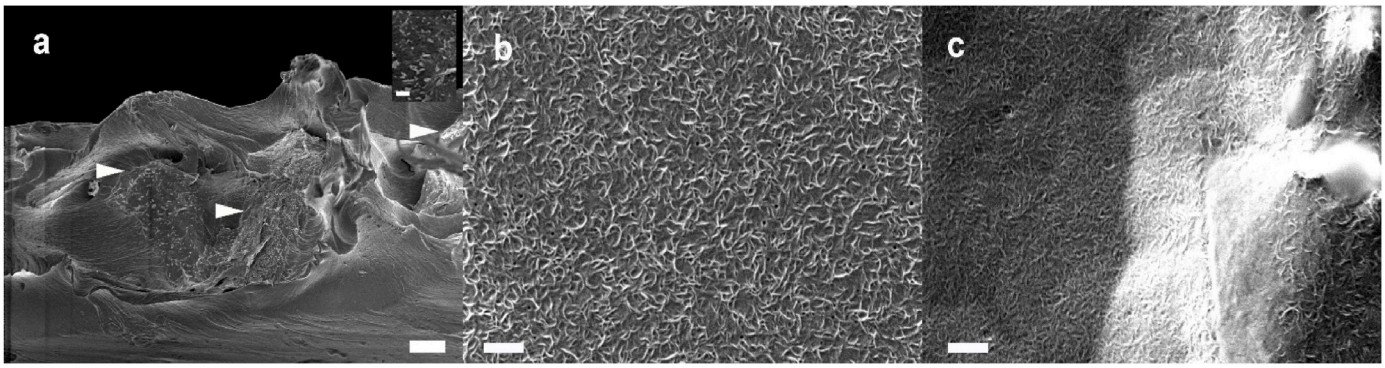

Fig. 2. a) FESEM image of the cross-section of Blend FSI10. The inset shows a detail of the microstructure of one of the dispersed aggregates (see text). The scale bar corresponds to 5 μm in the main picture and to 1 μm in the inset. The arrows indicate PEDOT:PSS aggregates in the interior of the sample. FESEM image of the surface of Blend FSI10 (b) and Blend FSI40 (c). The scale bar in b) and c) represents 1 μm.

$$F(\beta) = F_{EA} \times \left(\frac{AH'_{\beta}}{AH'_{\beta} + AH'_{\gamma}} \right) \times 100\% \quad (2)$$

$$F(\gamma) = F_{EA} \times \left(\frac{AH'_{\gamma}}{AH'_{\beta} + AH'_{\gamma}} \right) \times 100\% \quad (3)$$

where, AH'_{β} and AH'_{γ} are the absorbance differences between the peak at 1275 cm^{-1} and 1260 cm^{-1}, and the peak at 1234 cm^{-1} and 1225 cm^{-1}, respectively.

The dielectric response ($\varepsilon^* = \varepsilon' - i\varepsilon''$) was determined using an impedance analyzer Alpha-S in the frequency range from 0.1 Hz to 1 MHz. The isothermal measurements were carried out from −120 °C to 150 °C (thermal stability: 0.5 °C) in 5 °C steps, the temperature control being ensured with a Quatro Cryosystem from Novocontrol GmbH where the capacitance ($C = \varepsilon' \varepsilon_0 A/d$) and the loss factor ($tan\,\delta = \varepsilon''/\varepsilon'$) were measured in order to obtain the real, ε', and the imaginary, ε'', components of the dielectric function, ε_0 is the permittivity of vacuum (8.85×10^{-12} F m^{-1}), A is the electrode area (m^2) and d is the thickness of samples (m).

Circular gold electrodes with a diameter of 10 mm were sputtered onto both sides of each sample using a Polaron Coater SC502.

The complex conductivity, σ*, was calculated using equation (4):

$$\sigma^* = \sigma'(\omega) + i\sigma''(\omega) \quad (4)$$

where σ'(ω) and σ''(ω) are the real and imaginary components of the conductivity, respectively. σ' is given by equation (5), and σ'' is given by equation (6):

$$\sigma'(\omega) = \varepsilon_0 \omega \varepsilon''(\omega) \quad (5)$$

$$\sigma''(\omega) = \varepsilon_0 \omega \varepsilon'(\omega) \quad (6)$$

where ε_0 (8.85×10^{-12} Fm^{-1}) is the permittivity of free space and ω is the angular frequency.

The complex electric modulus M^* is defined as the inverse of the complex relative permittivity, $\varepsilon^*(\omega)$:

$$M^*(\omega) = {}^1/_{\varepsilon^*(\omega)} = M'(\omega) + iM''(\omega) \quad (7)$$

Therefore, the real part of the complex electric modulus is obtained using:

$$M'(\omega) = \frac{\varepsilon'(\omega)}{\varepsilon'^2(\omega) + \varepsilon''^2(\omega)} \quad (8)$$

and the imaginary part of the complex electric modulus is obtained using:

$$M''(\omega) = \frac{\varepsilon''(\omega)}{\varepsilon'^2(\omega) + \varepsilon''^2(\omega)} \quad (9)$$

where ε' and ε'' represent the real and imaginary components of the dielectric function.

3. Results and discussion

3.1. Morphological analysis

The preparation of the PVDF/PEDOT:PSS/IL films by solvent-casting results in films in which the two faces are not identical in terms of morphology. One of the faces is formed in contact with the glass and the other in the air, in which the spherulite structure is seen more clearly. Fig. 1 shows that the surface becomes rougher as the amount of PEDOT:PSS/IL in the sample increases.

The PVDF spherulites are clearly shown in all compositions, but their size decreases with the content of PEDOT:PSS and IL, as can be seen comparing the images in Fig. 1b with 1 d, 1f, and 1 h. It seems that there are in the interior aggregates with angular shapes that form ridges on the surface, but above these ridges the spherulites are visible, with the characteristic morphology of PVDF. These results suggest that aggregates of PEDOT:PSS had been separated in an initial phase of film formation and then, when the PVDF crystallizes, a layer is formed covering them. This could be due to the fact that when mixing the solutions of PEDOT:PSS/IL in ethanol with that of PVDF in DMF, the PEDOT:PSS precipitates forming these aggregates because its solubility in the mixture of ethanol and DMF has decreased compared to pure ethanol.

It can be observed (Fig. 1), that the PEDOT:PSS aggregates increase in number in the blend FSI series as the amount of PEDOT:PSS increases, as expected, but they are also clearly larger in size in the mixture with [C2mpyr][TFSI] than in the mixture with [C2mpyr][FSI] as evidenced by comparing Fig. 1g and h.

The size of the spherulites shown at the surface depends essentially on the nucleation of the crystals. After the formation of a stable crystalline core, the spherulite grows radially, incorporating chains of liquid PVDF, until it meets the front of another spherulite. This means that when few crystallization nuclei are formed, the resulting spherulites are large, as seen in pure PVDF where they easily reach 10 μm in diameter. On the contrary, when the nucleation is higher, the resulting spherulites are smaller because many spherulites are growing at the same time. Since heterogeneous nucleation (the one in which crystal nuclei form in two dimensions on the surface of an impurity), is more likely than homogeneous nucleation (the one that forms in three dimensions within the liquid), the results presented in Fig. 1 seem to indicate that the PEDOT:PSS or IL aggregates are acting as agents that facilitate the PVDF nucleation, and therefore they were formed before the PVDF

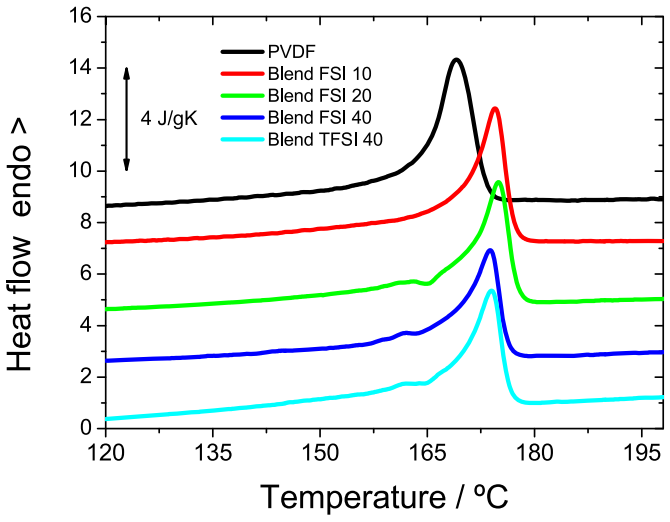

Fig. 3. - DSC heating thermogram in the temperature region of PVDF melting (second heating scan) for neat PVDF and PVDF/PEDOT:PSS/IL blends incorporating different IL contents.

crystallization started.

It is expected that when mixing the solutions of PEDOT:PSS in ethanol and PVDF in DMF the separation between the two polymeric components is not complete and some of the PEDOT:PSS remains mixed with the PVDF in the DMF solution. This amount of PEDOT:PSS must be segregated when the PVDF crystallises.

A hypothesis that is further confirmed by Fig. 2a) in which the internal distribution of PEDOT:PSS and IL can be observed. These fillers are distributed in big lumps rather than homogeneously throughout the PVDF matrix, corresponding to the regions marked with arrows, where homogenously distributed light-colored dots can be observed, corresponding to precipitated lumps of PEDOT in which the IL is uniformly dispersed (light-colored dots). A detail of the microstructure of these lumps is shown in the inset of Fig. 2a.

The curious topography observed at high magnifications on the film surface must be caused by this segregation of PEDOT:PSS migrating to the surface. Fig. 2b shows the image of Blend FSI10 sample in a flat zone of the surface. This topography showing small worms is also shown to a lesser extent in blends with higher PEDOT:PSS content, Fig. 2c showing the case of Blend FSI40.

When the surface is viewed at even higher magnifications, it can be observed that the surface of the PVDF spherulites has a particular structure, very different from that of pure PVDF. It is difficult to speculate on the origin of these structures in the form of small lines that appear in the FESEM image in light color. It could be due to a change in the structure of the PVDF lamellae due to the presence of IL, which would cause the phase in which the PVDF crystallizes to change, or the IL itself to be secreted during the growth of the PVDF crystals, remaining in inter-lamella regions (Fig. 2b and c).

3.2. Thermal analysis

The DSC heating thermograms of the blends (Fig. 3) show only the melting endotherm peak of PVDF due to the amorphous character of pure PEDOT:PSS. The second heating scan is shown, in which PVDF have been crystallized on cooling at 20 °C/min. There is no clear trend in the Blend FSI series, but there are two notable facts. On the one hand, the temperature of the PVDF melting peak does not depend on the PEDOT:PSS content of the blend, which suggests that indeed, as suggested in the

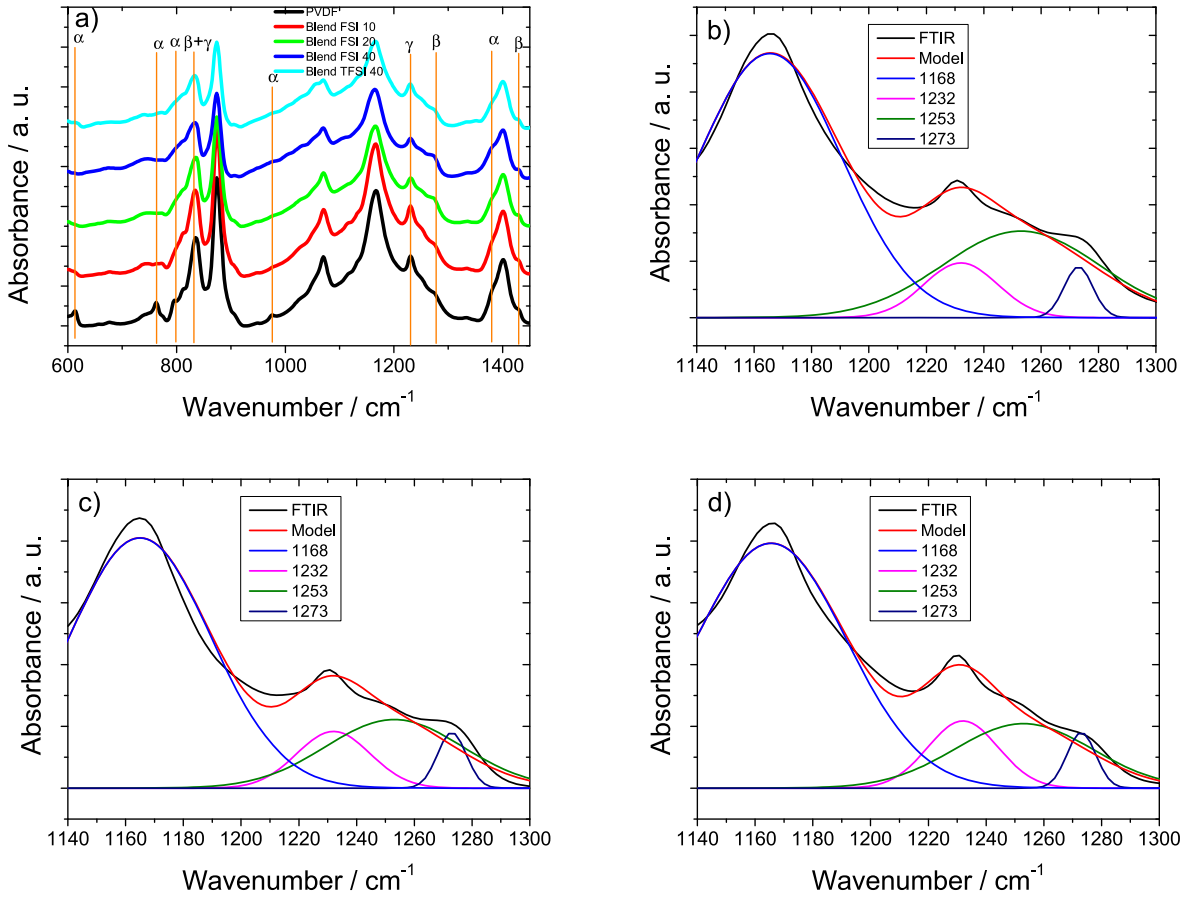

Fig. 4. - (a) FTIR spectra of all blend samples and deconvolution for BlendFSI20 (b), Blend FSI40 (c) and BlendTFSI40 (d) samples.

Table 2
- Percentage of the three crystalline phases of PVDF for the blend samples.

%	PVDF	BlendFSI10	BlendFSI20	BlendFSI40	BlendTFSI40
α-phase	34	0	0	0	0
β-phase	16	35	47	54	45
γ-phase	50	65	53	46	55

Table 3
- Real component of the electrical conductivity (σ') of neat PVDF and PVDF/PEDOT:PSS/IL blends incorporating different IL contents.

	PVDF	BlendFSI10	BlendFSI20	BlendFSI40	BlendTFSI40
σ'/S. cm^{-1}	2,25 × 10^{-12}	5,94 × 10^{-9}	7,08 × 10^{-6}	1,80 × 10^{-6}	5,54 × 10^{-5}

morphology section, the PEDOT:PSS at least partially precipitates in the form of aggregates when its solution in ethanol is mixed with the PVDF solution. If it were not so, a cryoscopic decrease would have been appreciated due to the mixing of the two polymeric components of the blend. All the mixtures show that the melting peak is 6 °C above that of neat PVDF. As it will be presented below, FTIR probes that PVDF crystallizes in the blend in a different crystalline phase than in the pure PVDF film what justifies the shift in the melting peak.

3.3. Polymer phase analysis

Fig. 4a shows the FTIR spectra for the different blend samples in order to evaluate whether IL or PEDOT:PSS induce homogeneous crystallization of PVDF in the electroactive phase. Although the interaction of PVDF with the IL may be homogeneous during crystallization, the

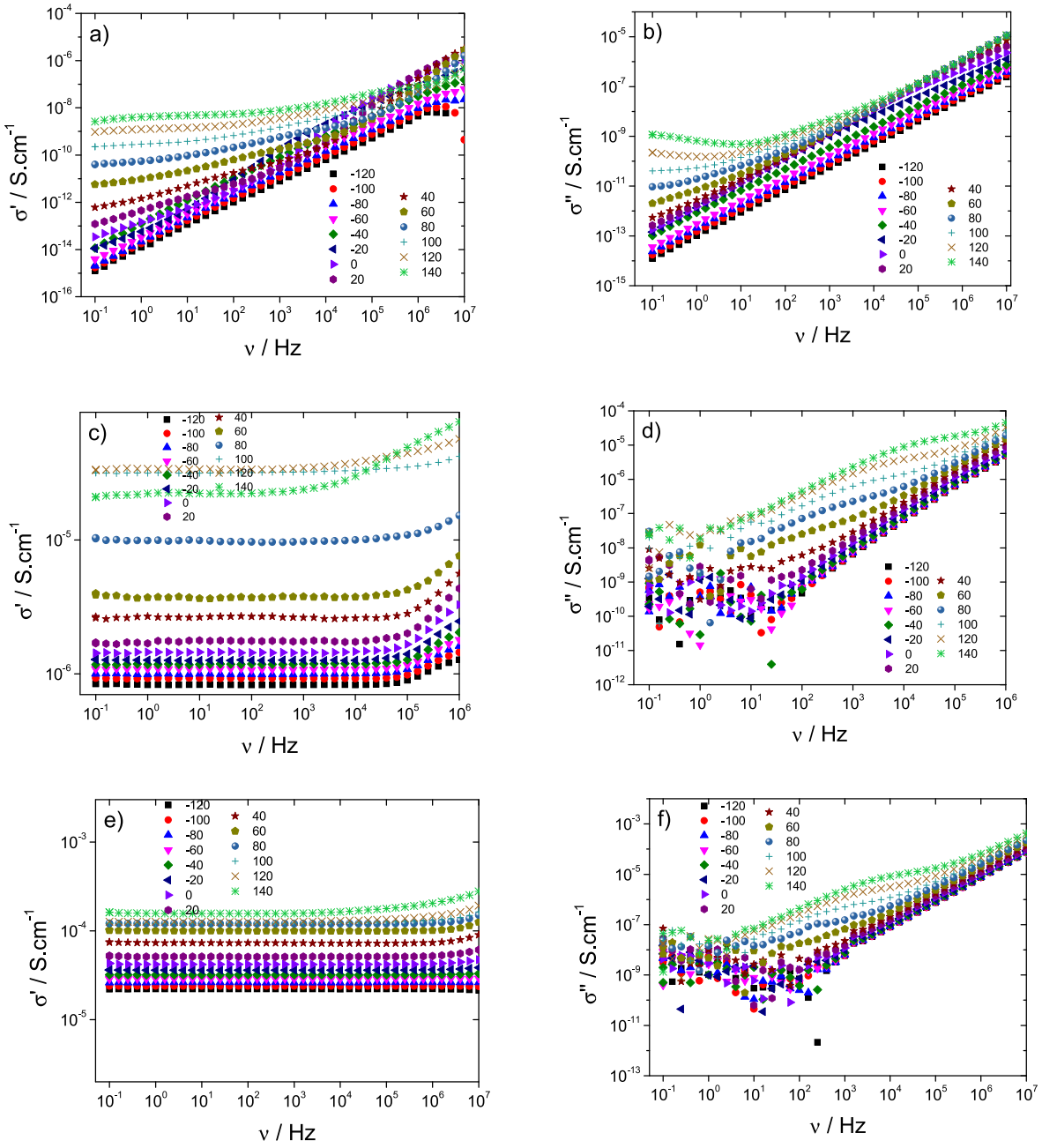

Fig. 5. - Real (σ') and imaginary part (σ'') of the electrical conductivity as a function of frequency at different temperatures for neat PVDF (a and b), BlendFSI40 (c and d) and BlendTFSI40 (e and f).

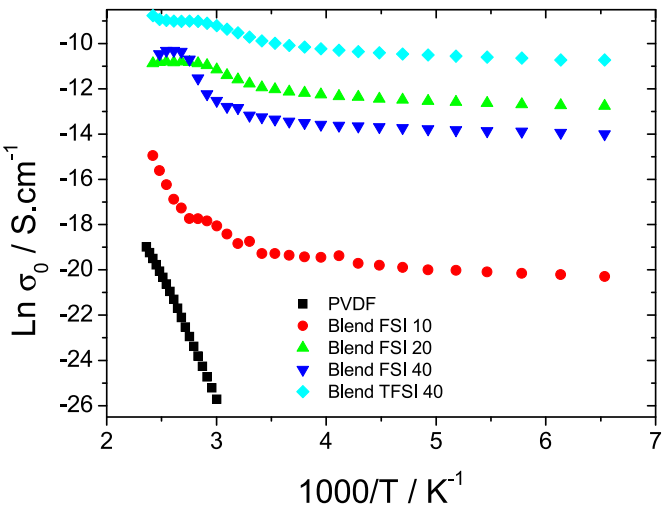

Fig. 6. d. c. Electrical conductivity (obtained from the plateau of σ′) for the different blend samples.

interaction with PEDOT:PSS would occur at the interfaces with the aggregates that have been formed.

Analyzing Fig. 4a, it is observed absorption bands at 614, 763, 795, and 975 cm^{-1}, which correspond to the α-phase of PVDF [45], the intensity of these bands depending on the amount of PEDOT:PSS/IL. Also, absorption bands at 840 and 1275 cm^{-1}, corresponding to the β-phase of PVDF, are detected. Furthermore, the vibration peaks at 1234 and 840 cm^{-1}, characteristic of the γ phase of PVDF can be observed. The quantification of the three phases was calculated from equations (1)–(3) through the deconvolution of the peaks at 1300 to 1140 cm^{-1} as shown in Fig. 4b to d. The figure shows the deconvolution for the BlendFSI20, Blend FSI40 and BlendTFSI40 samples (the remaining samples show a similar behavior). Table 2 shows the quantification of the three PVDF phases for the blend samples, as the presence of the three crystalline phases is verified in all blend samples.

The increase in β phase content with the addition of IL is due to the electrostatic dipole-ion interactions between the PVDF polymer chains and the IL, originated by the interaction of anions in the IL and dipoles of the polymer chains [46].

A decrease in the γ phase and an increase in the β phase content are observed as the IL content increases in the blend samples with FSI, while the TFSI seems to promote less crystallization in the polar β phase than the FSI with the same content (40 %). The results indicate that the lower content of IL in the Blend10FSI mixture is the one that most impacts PVDF crystallization, promoting a decrease in the α phase and an increase in the β and γ phases, which could explain the differences in the surface morphology and the thermal behaviour (DSC second scan). Higher IL contents cause the α phase fraction to return to the values of neat PVDF.

3.4. Conductivity formalism analysis

The real (σ′) and imaginary (σ′′) parts of the electrical conductivity for all blend samples are shown in Fig. 5 and S1 in supplementary information. Table 3 shows the real component of the electrical conductivity (σ′) at 1 kHz and room temperature.

Regardless of the sample, it is observed that σ′ and σ′′ increase with increasing temperature and frequency. Both σ′ and σ′′ increase as a function of frequency due to the electrode polarization, which represents the accumulation of ionic charge carriers at the electrode-sample interface [47].

The electrical behavior change with respect to pristine PVDF with the

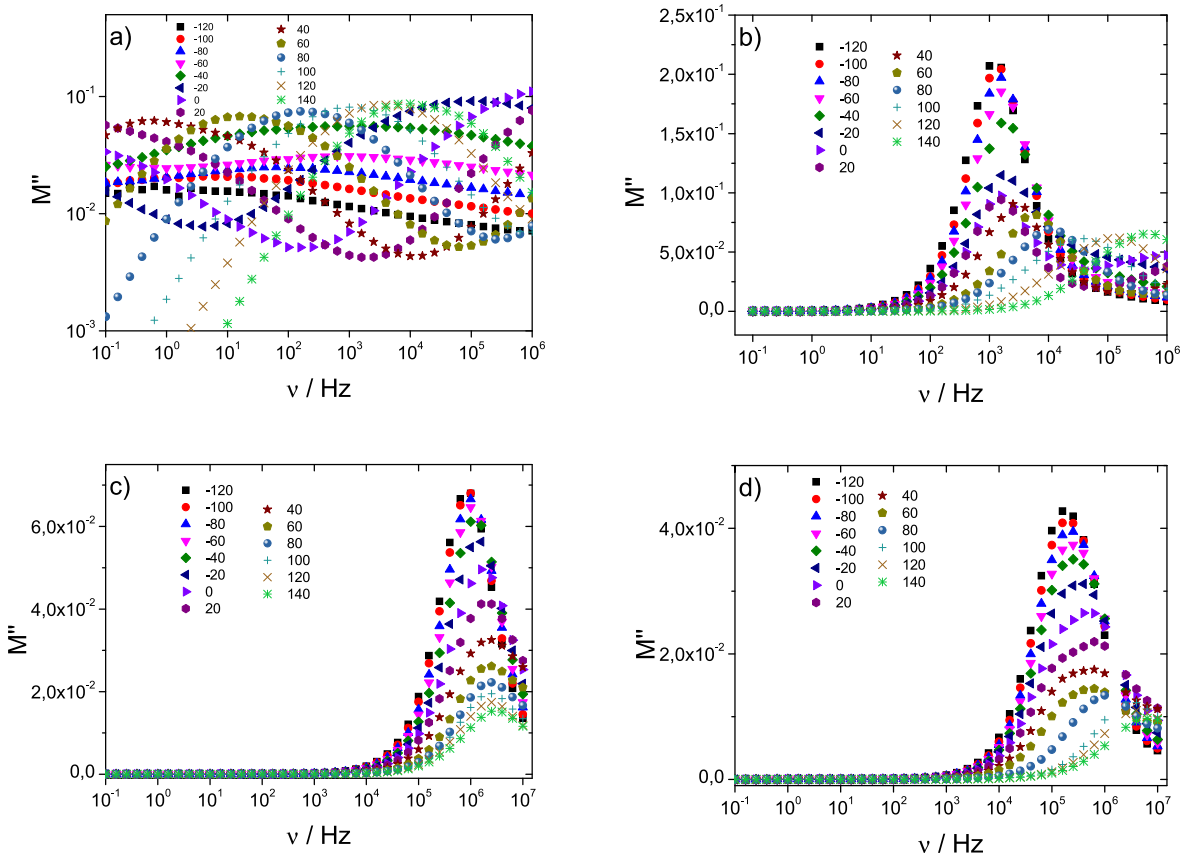

Fig. 7. - Isothermal spectra of the imaginary part of the complex modulus (M″) for neat PVDF (a), and BlendFSI10 (b), BlendFSI20 (c) and BlendFSI40 (d).

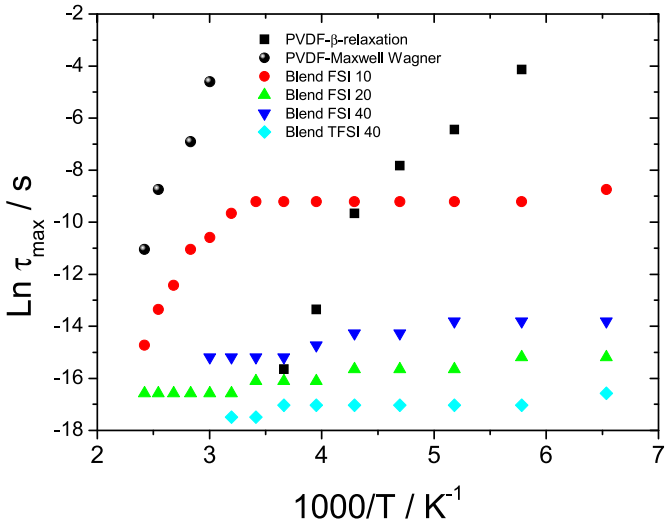

Fig. 8. - Relaxation times obtained from the maxima of M″ for the blend samples.

addition of only 7 % PEDOT:PSS and 3 % IL is highly noticeable, as seen in Fig. 5a (PVDF) and S1 a-b) in supplementary information (Blend FSI10). The combination of the conductive polymer, even in the form of micrometric aggregates, and the IL makes the sample to present higher conductivity in a very wide temperature range, even at very low temperatures.

The BlendFSI20 sample (Fig. S1 c and d) further extends the dc conductivity plateau and increases the dc conductivity value by about 3 orders of magnitude (Fig. 5). Then, a further increase in PEDOT:PSS content and the IL no longer increases the dc conductivity. The sample with 40 wt% PEDOT:PPS + IL presents slightly lower conductivity values (Fig. 5c and d). This result suggests that with the BlendFSI20 sample, percolation of the conductive particles has been achieved. BlendFSI40 shows a lower conductivity due to the presence of aggregates, indicating that the percolation should be between 20 and 40 wt%.

The blend containing IL [C2mpyr][TFSI] (Fig. 5e and f) seems to have a somewhat higher conductivity than that containing [C2mpyr][FSI] (Fig. 5c and d), which can be attributed to the different morphology adopted by the PEDOT:PSS aggregates.

Fig. 6 shows the dc conductivity as a function of temperature for the different blend samples showing a thermally activated behavior described by the charge transport mechanism. It can be observed that dc conductivity increases with the increase of PEDOT:PSS/IL content due to higher number of charge carriers in the polymer matrix [48].

3.5. Electric modulus formalism

The dielectric permittivity curves do not present relevant features due to the superimposition of the large dc conductivity of the samples. To analyze the electrical behavior in greater depth, the electric modulus formalism has been used, since it transforms the conductivity-related process into a relaxation peak and also limits the effect of the electrode polarization [47,49]. Fig. 7 shows the imaginary part of the complex modulus for all blend samples between −120 °C and 140 °C.

In neat PVDF (Fig. 7a), the isotherms of M″ show two relaxation processes. The low-temperature, very wide one, corresponds to the main dipolar relaxation, associated with the glass transition of the amorphous phase. It shifts towards high frequencies as the temperature increases while it grows in intensity. In Fig. 7a, this process can be particularly well identified in the curve corresponding to −20 °C. A somewhat narrower peak can be observed at higher temperatures (from 40 °C onwards), which also shifts towards higher frequencies as the temperature increases. This peak is associated with an interfacial or Maxwell-Wagner polarization phenomenon due to the accumulation of electric charge carriers at the interfaces between the crystals and the amorphous phase.

In this representation of M″, the drastic change in dielectric behavior is again observed when adding a small amount of PEDOT:PSS and IL. In the BlendFSI10 mixture, although some remains of the PVDF Maxwell-Wagner peak are observed, an overlapping peak appears whose position hardly depends on temperature and which can be associated with the contribution of the dc conductivity plateau observed in Fig. 6. The peak appears in the samples BlendFSI20 and BlendFSI40 and BlendTFSI40 in somewhat different positions, since the dc conductivity is different in some samples but with an analogous behavior.

In this temperature range of the M″ spectra, the observed peak which corresponds to the conductivity behavior is slightly shifted to higher frequencies with increasing temperature. An apparent relaxation time has been defined as the reciprocal frequency of the maximum of M'' ($\tau_{max} = 1/\omega_{max}$) where the temperature dependence of the relaxation times for all blend samples is shown in Fig. 8.

Fig. 8 shows that relaxation time decreases with increasing the PEDOT:PSS/IL amount due to the increase of the Maxwell-Wagner effect (clearly noticeable in neat PVDF and BlendFSI10 samples) and the dc conductivity induced by the presence of the IL.

In order to evaluate the different electrical processes/contributions for these blend samples, the Cole-Cole arcs for the electric modulus formalism are shown in Fig. 9 for the temperature range between −120 and 120 °C, where the different relaxation phenomena can be more clearly identified.

For neat PVDF, Fig. 9a shows two arcs corresponding to the β-relaxation and Maxwell-Wagner process that depend on the temperature. However, the blend sample BlendFSI40 (Fig. 9b) shows only a single arc (the rest of the blend samples show a similar behavior), which

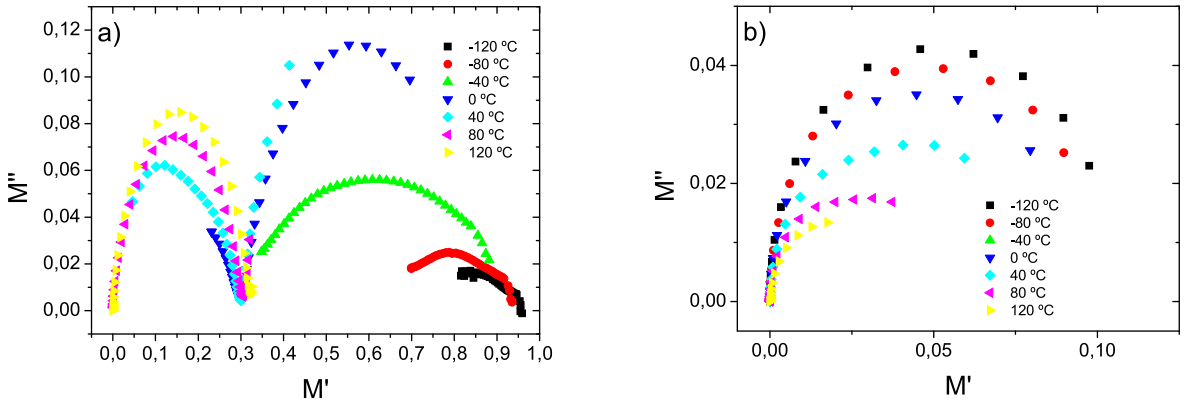

Fig. 9. - Cole-Cole plots of the electric modulus for neat PVDF (a) and BlendFSI40 (b).

indicate that the conductivity is the main dominant process, overlapping the β-relaxation of PVDF and interfacial polarization.

4. Conclusions

The morphological, thermal, polymer phase and electrical properties of PVDF/PEDOT:PSS/IL blends with different PEDOT:PSS/IL contents (10 wt%≤ PEDOT:PSS/IL ≤ 40 wt%) were obtained and analyzed to determine the influence of PEDOT:PSS/IL on the crystallization kinetics of the polymer matrix and on the ionic conductivity and electrical modulus formalisms. The morphology of PVDF is affected by the inclusion of PEDOT:PSS/IL, leading to a decrease in the spherulite microstructure. It is observed that PEDOT:PSS acts as a nucleation agent for polymer crystallization. The interaction of PEDOT:PSS and PVDF occurs at the interfaces, leading to the homogeneous crystallization of PVDF. Furthermore, β-phase and γ-phase PVDF content increases with increasing PEDOT:PSS/IL within the blends, demonstrating its interaction and compatibility with the PVDF polymer matrix. The inclusion of PEDOT:PSS/IL leads to an increase in the ionic conductivity value of the blend. The electrical conductivity corresponds to a thermally activated process described by the charge transport mechanism in which PEDOT:PSS/IL content increases the charge carriers number. The percolation threshold for electrical conduction is found between 20 wt% and 40 wt% filler content. This new blend based on PVDF and PEDOT:PSS-IL allows to tailor PVDF polymer phase and electrical conductivity characteristics, being suitable for applications based on the ionic conductivity of the materials, such as sensors, soft bending actuators and energy storage devices.

The development of functional blend materials with tailored electrical conductivity based on conductive polymers and ionic liquids and the understanding of their physical-chemical properties is essential for the application of these materials in the aforementioned areas.

CRediT authorship contribution statement

Luis Amaro Martins: Investigation, Methodology, Validation, Writing - original draft, Writing - review & editing. **Laura Teruel Biosca:** Investigation, Methodology, Validation, Writing - original draft, Writing - review & editing. **Roser Sabater i Serra:** Formal analysis, Investigation, Methodology, Validation, Writing - original draft, Writing - review & editing. **Andreu Andrio Balado:** Investigation, Methodology, Validation, Writing - original draft, Writing - review & editing. **José Antonio Gómez-Tejedor:** Investigation, Methodology, Validation, Writing - original draft, Writing - review & editing. **Daniela M. Correia:** Investigation, Methodology, Validation, Writing - original draft, Writing - review & editing. **Liliana Fernandes:** Investigation, Methodology, Validation, Writing - original draft, Writing - review & editing. **Carlos M. Costa:** Formal analysis, Investigation, Methodology, Validation, Writing - original draft, Writing - review & editing. **Senentxu Lanceros-Méndez:** Conceptualization, Formal analysis, Funding acquisition, Methodology, Project administration, Resources, Validation, Writing - original draft, Writing - review & editing. **José Luis Gomez Ribelles:** Conceptualization, Formal analysis, Investigation, Methodology, Validation, Writing - original draft, Writing - review & editing. **Isabel Tort-Ausina:** Formal analysis, Investigation, Methodology, Validation, Writing - original draft, Writing - review & editing.

Declaration of competing interest

The authors declare that they have no known competing financial interests or personal relationships that could have appeared to influence the work reported in this paper.

Data availability

Data will be made available on request.

Acknowledgements

The authors thank the Fundação para a Ciência e Tecnologia (FCT) for financial Support under the framework of Strategic Funding UIDB/04650/2020, UID/FIS/04650/2020, UID/EEA/04436/2020, and UID/QUI/0686/2020 and under projects, MIT-EXPL/TDI/0033/2021, 2022.03931. PTDC and POCI-01-0247-FEDER-046985 funded by national funds through FCT and by the ERDF through the COMPETE2020—Programa Operacional Competitividade e Internacionalização (POCI). The authors also thank the FCT for financial support under grant SFRH/BD/145345/2019 (L.F.), and FCT investigator contracts 2020.02915. CEECIND (D.M.C), and 2020.04028. CEECIND (C.M.C.). Financial support from the Basque Government Industry Department under the ELKARTEK program is acknowledged. The authors thank for technical and human support provided by SGIker (UPV/EHU/ERDF, EU).

This work was funded by the Spanish State Research Agency (AEI) through the Grant number PID2022-138572OB-C41 and PID2022-138572OB-C42. CIBER-BBN is an initiative funded by the VI National R&D&I Plan 2008–2011, Iniciativa Ingenio 2010, Consolider Program. CIBER Actions were financed by the Instituto de Salud Carlos III with assistance from the European Regional Development Fund. The Microscopy Service of the UPV (Universitat Politècnica de València) is gratefully acknowledged for helping with FESEM characterization.

Appendix A. Supplementary data

Supplementary data to this article can be found online at doi: mmcdoino.

References

[1] G. Aktas Eken, M. Hayri Acar, Chapter 9 - PVDF-based shape memory materials, in: B. Ameduri, S. Fomin (Eds.), Opportunities for Fluoropolymers, Elsevier, 2020, pp. 247–274.
[2] A. Kelly, R. Davidson, K. Uchino, N. Shanmuga Priya, M. Shanmugasundaram, 7.18 smart composite materials systems, in: P.W.R. Beaumont, C.H. Zweben (Eds.), Comprehensive Composite Materials II, Elsevier, Oxford, 2018, pp. 358–363.
[3] M.R. Aguilar, J. San Román, 1 - introduction to smart polymers and their applications, in: M.R. Aguilar, J. San Román (Eds.), Smart Polymers and Their Applications, Woodhead Publishing, 2014, pp. 1–11.
[4] M. Falahati, P. Ahmadvand, S. Safaee, Y.-C. Chang, Z. Lyu, R. Chen, et al., Smart polymers and nanocomposites for 3D and 4D printing, Mater. Today 40 (2020) 215–245.
[5] C.M. Costa, V.F. Cardoso, P. Martins, D.M. Correia, R. Gonçalves, P. Costa, et al., Smart and multifunctional materials based on electroactive poly(vinylidene fluoride): recent advances and opportunities in sensors, actuators, energy, environmental, and biomedical applications, Chem. Rev. 123 (19) (2023) 11392–11487.
[6] C. Ribeiro, C.M. Costa, D.M. Correia, J. Nunes-Pereira, J. Oliveira, P. Martins, et al., Electroactive poly(vinylidene fluoride)-based structures for advanced applications, Nat. Protoc. 13 (4) (2018) 681–704.
[7] L.C. Fernandes, D.M. Correia, E. Fernández, M. Tariq, J.M.S.S. Esperança, S. Lanceros-Méndez, Design of ionic-liquid-based hybrid polymer materials with a magnetoactive and electroactive multifunctional response, ACS Appl. Mater. Interfaces 12 (37) (2020) 42089–42098.
[8] R. Mitra, B. Sheetal Priyadarshini, A. Ramadoss, U. Manju, Stretchable polymer-modulated PVDF-HFP/TiO2 nanoparticles-based piezoelectric nanogenerators for energy harvesting and sensing applications, Mater. Sci. Eng. B: Solid-State Materials for Advanced Technology (2022) 286.
[9] D.M. Correia, J.C. Barbosa, J.P. Serra, R.S. Pinto, L.C. Fernandes, C.R. Tubio, et al., Comparative assessment of ionic liquid-based soft actuators prepared by film casting versus direct ink writing, Adv. Eng. Mater. 23 (10) (2021).
[10] Z. Hao, S. Song, B. Li, Q.X. Jia, T. Zheng, Z. Zhang, A solvent driven dual responsive actuator based on MOF/polymer composite, Sensor. Actuator. B Chem. (2022) 358.
[11] J.A. Orkwis, A.K. Wolf, Z.J. Mularczyk, A.E. Bryan, C.S. Smith, R. Brown, et al., Mechanical stimulation of a bioactive, functionalized PVDF-TrFE scaffold provides electrical signaling for nerve repair applications, Biomater. Adv. (2022) 140.
[12] X. Meng, Q. Li, Z. Hu, M. Guo, Microfluidic fabrication of β-phase enriched poly (vinylidene fluoride) microfibers toward flexible piezoelectric sensor, J. Polym. Sci. 60 (11) (2022) 1718–1726.
[13] Y. Yu, J. Guo, L. Sun, X. Zhang, Y. Zhao, Microfluidic Generation of Microsprings with Ionic Liquid Encapsulation for Flexible Electronics, vol. 2019, Research (Wash D C), 2019, 6906275.

[14] M. Golmohammadi, A.A. Sabbagh Alvani, H. Sameie, B. Mei, R. Salimi, D. Poelman, et al., Photocatalytic nanocomposite membranes for environmental remediation, Nanotechnology 33 (46) (2022).
[15] J.M. Queirós, H. Salazar, A. Valverde, G. Botelho, R. Fernández de Luis, J. Teixeira, et al., Reusable composite membranes for highly efficient chromium removal from real water matrixes, Chemosphere (2022) 307.
[16] R.S. Pinto, J.P. Serra, J.C. Barbosa, R. Gonçalves, M.M. Silva, S. Lanceros-Méndez, et al., Direct-ink-writing of electroactive polymers for sensing and energy storage applications, Macromol. Mater. Eng. 306 (11) (2021).
[17] X. Zhang, W. Yang, H. Zhang, M. Xie, X. Duan, PEDOT:PSS: from conductive polymers to sensors, Nanotechnology and Precision Engineering 4 (4) (2021), 045004.
[18] Y. Yang, H. Deng, Q. Fu, Recent progress on PEDOT:PSS based polymer blends and composites for flexible electronics and thermoelectric devices, Mater. Chem. Front. 4 (11) (2020) 3130–3152.
[19] X. Fan, W. Nie, H. Tsai, N. Wang, H. Huang, Y. Cheng, et al., PEDOT:PSS for flexible and stretchable electronics: modifications, strategies, and applications, Adv. Sci. 6 (19) (2019), 1900813.
[20] A. Srivastava, D. Sharma, P. Kumari, M. Dutta, S.K. Srivastava, Highly efficient PEDOT:PSS/silicon hybrid solar cells via effective surface microengineering of low-c aaaost solar-grade silicon wafers, ACS Appl. Energy Mater. 4 (4) (2021) 4181–4198.
[21] R.K. Sharma, A. Srivastava, P. Kumari, D. Sharma, J.S. Tawale, V.V. Agrawal, et al., Graphene oxide modified PEDOT:PSS as an efficient hole transport layer for enhanced performance of hybrid silicon solar cells, Surface. Interfac. 36 (2023), 102577.
[22] A. Srivastava, R.K. Sharma, D. Sharma, P. Kumari, V.V. Agrawal, S.K. Srivastava, Influence of alcoholic polar surfactants on PEDOT:PSS for enhanced performance of organic/Si hybrid solar cell, Surface. Interfac. 38 (2023), 102822.
[23] D. Sharma, A. Srivastava, J.S. Tawale, P. Prathap, S.K. Srivastava, High efficiency flexible PEDOT:PSS/silicon hybrid heterojunction solar cells by employing simple chemical approaches, J. Mater. Chem. C 11 (39) (2023) 13488–13502.
[24] S. Khasim, A. Pasha, M. Lakshmi, P. Chellasamy, M. Kadarkarai, A.A.A. Darwish, et al., Post treated PEDOT-PSS films with excellent conductivity and optical properties as multifunctional flexible electrodes for possible optoelectronic and energy storage applications, Opt. Mater. 125 (2022), 112109.
[25] L. Liu, S. Choi, PEDOT:PSS/MnO2/CNT ternary nanocomposite anodes for supercapacitive energy storage in cyanobacterial biophotovoltaics, ACS Appl. Energy Mater. 3 (10) (2020) 10224–10233.
[26] M. Solazzo, M.G. Monaghan, Structural crystallisation of crosslinked 3D PEDOT:PSS anisotropic porous biomaterials to generate highly conductive platforms for tissue engineering applications, Biomater. Sci. 9 (12) (2021) 4317–4328.
[27] A. Magaz, B.F. Spencer, J.G. Hardy, X. Li, J.E. Gough, J.J. Blaker, Modulation of neuronal cell affinity on PEDOT–PSS nonwoven silk scaffolds for neural tissue engineering, ACS Biomater. Sci. Eng. 6 (12) (2020) 6906–6916.
[28] Y. Liang, A. Offenhäusser, S. Ingebrandt, D. Mayer, PEDOT:PSS-Based bioelectronic devices for recording and modulation of electrophysiological and biochemical cell signals, Adv. Healthcare Mater. 10 (11) (2021), 2100061.
[29] G. Li, C.F. Guo, PEDOT:PSS-based intrinsically soft and stretchable bioelectronics, Soft Sci. 2 (2) (2022) 7.
[30] N. Terasawa, K. Asaka, High-Performance PEDOT:PSS/Single-Walled carbon nanotube/ionic liquid actuators combining electrostatic double-layer and faradaic capacitors, Langmuir 32 (28) (2016) 7210–7218.
[31] Y. Yuan, C. Tian, J. Liu, PEDOT surface modified PVDF filtration membrane for conductive membrane preparation and fouling mitigation, J. Environ. Chem. Eng. 9 (3) (2021), 105212.
[32] Y. Wen, J. Xu, Scientific importance of water-processable PEDOT–PSS and preparation, challenge and new application in sensors of its film electrode: a review, J. Polym. Sci. Polym. Chem. 55 (7) (2017) 1121–1150.
[33] A. Liu, P. Kovacik, N. Peard, W. Tian, H. Goktas, J. Lau, et al., Monolithic flexible supercapacitors integrated into single sheets of paper and membrane via vapor printing, Adv. Mater. 29 (19) (2017), 1606091.
[34] M. Döbbelin, R. Marcilla, M. Salsamendi, C. Pozo-Gonzalo, P.M. Carrasco, J. A. Pomposo, et al., Influence of ionic liquids on the electrical conductivity and morphology of PEDOT:PSS films, Chem. Mater. 19 (9) (2007) 2147–2149.
[35] A. de Izarra, S. Park, J. Lee, Y. Lansac, Y.H. Jang, Ionic liquid designed for PEDOT:PSS conductivity enhancement, J. Am. Chem. Soc. 140 (16) (2018) 5375–5384.
[36] A. de Izarra, C. Choi, Y.H. Jang, Y. Lansac, Ionic liquid for PEDOT:PSS treatment. Ion binding free energy in water revealing the importance of anion hydrophobicity, J. Phys. Chem. B 125 (7) (2021) 1916–1923.
[37] S. Kee, N. Kim, H. Park, B.S. Kim, M.Y. Teo, S. Lee, et al., Tuning the mechanical and electrical properties of stretchable PEDOT:PSS/ionic liquid conductors, Macromol. Chem. Phys. 221 (23) (2020), 2000291.
[38] M. Jangra, S. Dam, A. Thakur, S. Hussain, Modulating the conductivity of free-standing, flexible composite films of poly(vinylidene fluoride)/poly(3,4 ethyelenedioxythiophene):poly(styrelenesulfonate), Thin Solid Films 737 (2021), 138918.
[39] A. Closson, H. Richards, Z. Xu, C. Jin, L. Dong, J.X.J. Zhang, Method for inkjet-printing PEDOT:PSS polymer electrode arrays on piezoelectric PVDF-TrFE fibers, IEEE Sensor. J. 21 (23) (2021) 26277–26285.
[40] Z. Hu, J. Li, X. Wei, C. Wang, Y. Cao, Z. Gao, et al., Enhancing strain-sensing properties of the conductive hydrogel by introducing PVDF-TrFE, ACS Appl. Mater. Interfaces 14 (40) (2022) 45853–45868.
[41] M. Nan, D. Bang, S. Zheng, G. Go, B.A. Darmawan, S. Kim, et al., High-performance biocompatible nanobiocomposite artificial muscles based on ammonia-functionalized graphene nanoplatelets–cellulose acetate combined with PVDF, Sensor. Actuator. B Chem. 323 (2020), 128709.
[42] M.H. Chung, H.-J. Kim, S. Yoo, H. Jeong, K.-H. Yoo, Enhancement of triboelectricity based on fully organic composite films with a conducting polymer, RSC Adv. 12 (5) (2022) 2820–2829.
[43] G. Wang, H. Xia, X.-C. Sun, C. Lv, S.-X. Li, B. Han, et al., Actuator and generator based on moisture-responsive PEDOT: PSS/PVDF composite film, Sensor. Actuator. B Chem. 255 (2018) 1415–1421.
[44] P. Martins, A.C. Lopes, S. Lanceros-Mendez, Electroactive phases of poly (vinylidene fluoride): determination, processing and applications, Prog. Polym. Sci. 39 (4) (2014) 683–706.
[45] X. Cai, T. Lei, D. Sun, L. Lin, A critical analysis of the α, β and γ phases in poly (vinylidene fluoride) using FTIR, RSC Adv. 7 (25) (2017) 15382–15389.
[46] D.M. Correia, C.M. Costa, J.C. Rodríguez Hernández, I. Tort-Ausina, L.T. Biosca, C. Torregrosa Cabanilles, et al., Crystallization monitoring of semicrystalline poly (vinylidene fluoride)/1-Ethyl-3-methylimidazolium hexafluorophosphate [emim][PF6] ionic liquid blends, Cryst. Growth Des. 21 (8) (2021) 4406–4416.
[47] D.M. Correia, C.M. Costa, R. Sabater i Serra, J.A. Gómez Tejedor, L. Teruel Biosca, V. de Zea Bermudez, et al., Molecular relaxation and ionic conductivity of ionic liquids confined in a poly(vinylidene fluoride) polymer matrix: influence of anion and cation type, Polymer 171 (2019) 58–69.
[48] D.M. Correia, R. Sabater i Serra, J.A. Gómez Tejedor, V. de Zea Bermudez, A. Andrio Balado, J.M. Meseguer-Dueñas, et al., Ionic and conformational mobility in poly(vinylidene fluoride)/ionic liquid blends: dielectric and electrical conductivity behavior, Polymer 143 (2018) 164–172.
[49] C.M. Costa, A. Reizabal, R. Sabater i Serra, A.A. Balado, L. Pérez-Álvarez, J. L. Gómez Ribelles, et al., Broadband dielectric response of silk Fibroin/BaTiO3 composites: influence of nanoparticle size and concentration, Compos. Sci. Technol. 213 (2021), 108927.